OPEN

Energy efficiency in nanoscale synthesis using nanosecond plasmas

David Z. Pai[1,2,5], Kostya (Ken) Ostrikov[3,4], Shailesh Kumar[3,4], Deanna A. Lacoste[2], Igor Levchenko[3,4] & Christophe O. Laux[2]

[1]Department of Advanced Materials Science, Graduate School of Frontier Sciences, The University of Tokyo, 5-1-5 Kashiwanoha, Kashiwa-shi, Chiba 277 8562, Japan, [2]Laboratoire EM2C, CNRS UPR288, Ecole Centrale Paris, Grande Voie des Vignes, 92295 Châtenay-Malabry, France, [3]Plasma Nanoscience Centre Australia (PNCA), CSIRO Materials Science and Engineering, P.O. Box 218, Lindfield, New South Wales 2070 Australia, [4]Plasma Nanoscience@Complex Systems, School of Physics, The University of Sydney, Sydney, New South Wales 2006, Australia, [5]Département Fluides, Thermique et Combustion, Institut Pprime (CNRS UPR 3346, Université de Poitiers, ENSMA), bd Marie et Pierre Curie, Téléport 2, BP 30179F, 86962 Futuroscope, France.

We report a nanoscale synthesis technique using nanosecond-duration plasma discharges. Voltage pulses 12.5 kV in amplitude and 40 ns in duration were applied repetitively at 30 kHz across molybdenum electrodes in open ambient air, generating a nanosecond spark discharge that synthesized well-defined MoO_3 nanoscale architectures (i.e. flakes, dots, walls, porous networks) upon polyamide and copper substrates. No nitrides were formed. The energy cost was as low as 75 eV per atom incorporated into a nanostructure, suggesting a dramatic reduction compared to other techniques using atmospheric pressure plasmas. These findings show that highly efficient synthesis at atmospheric pressure without catalysts or external substrate heating can be achieved in a simple fashion using nanosecond discharges.

Efficiency in energy and matter consumption during synthesis is one of the Grand Science Challenges presently facing nanotechnology, which is expected to play a key role in the development of energy technologies critical for a sustainable future[1,2]. This is in addition to the drive to develop new nanofabrication processes that are economical at the industrial scale, environmentally friendly, and of high quality. Such innovation will ultimately require effective control of the energy and matter involved in nanoscale materials synthesis, which is the primary motivation for using the synthesis method introduced in this work. This technique is demonstrated here for the case of MoO_x nanostructures, which have potential applications in catalysis[3], charge storage[4], gas sensing[5], and field emission[6].

The existing methods for the production of MoO_x nanomaterials include hydrothermal processing[7] that can involve the use of templates[8], electrodeposition in solution[9], thermal evaporation followed by chemical vapor deposition (CVD)[6], thermal oxidation[10], flame synthesis[11], and plasma-based synthesis[12]. Wet chemistry processes are usually low-temperature and quite energy efficient but produce significant chemical waste, involve complicated steps for isolating products, and are more suited for the production of loose, unsupported nanoparticles[13]. Thermal evaporation methods typically must take place in vacuum environments or requires catalysts. Thermal and plasma CVD are more environmentally friendly but are less energy efficient due to higher temperatures and reduced pressures. Essentially, unnecessarily large quantities of energy and/or matter are mustered to synthesize small objects.

To address this problem, here we use the deterministic "building unit" approach[14], whereby only the required atoms should be produced from precursors before rapid delivery and incorporation into a nanoscale assembly with minimum loss and energy consumption. To be clear, we are concerned here with self-organized processes, as opposed to atom-by-atom manipulation, which is very inefficient in terms of time and cost. Figure 1(a) shows the deterministic approach in relation to the results to be presented in this work, namely metal-oxide nanostructures generated in open air. Ideally, metal and oxygen atoms would be produced and then consumed stoichiometrically. One efficient means of generating both species is to conduct electric current between two metal electrodes via a gas discharge in the inter-electrode gap. Metal atoms come via evaporation from the electrodes and the oxygen atoms via dissociation of O_2 in the gas phase. Thus, targeting the discharge energy towards efficient dissociation of O_2 is of primary interest. To produce a pure metal vapor, a high-current discharge can be efficiently used in which the current is localized in high-temperature spots on the electrode surface. In this case mainly pure metal ions are usually produced[15,16].
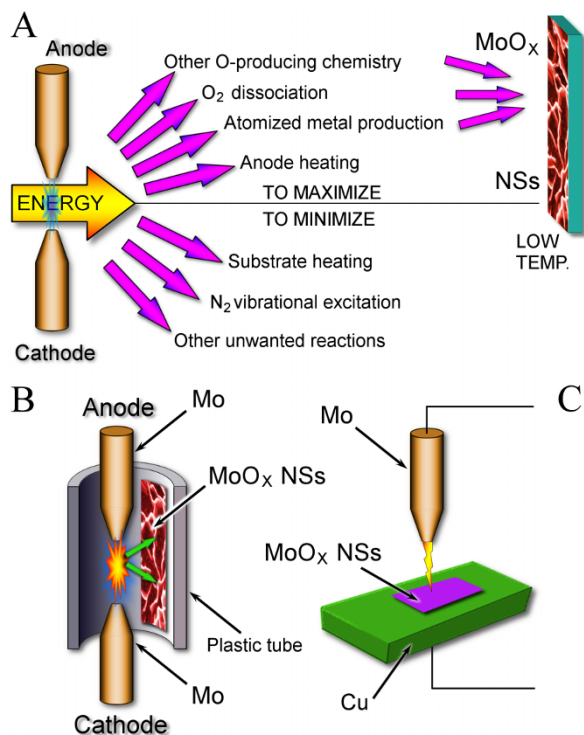
Figure 1 | **Schematics of the experimental setups for the deposition of MoO$_x$ nanostructures (NS) by nanosecond repetitively pulsed (NRP) spark discharges in open ambient air.** (a) The deterministic approach for energy-efficient nanoscale synthesis using atmospheric-pressure plasmas in air (b) The pin-to-pin electrode configuration for "remote deposition" in which the Mo electrodes act as a source of Mo, and the tube enclosing the electrodes is the substrate for the deposition of MoO$_x$, and (c) the pin-to-plate electrode configuration for "direct deposition" in which the pin electrode is the source of Mo, and the copper plate is the substrate.

Figure 2 | **Schematic of the characteristic times of nanosecond repetitively pulsed (NRP) discharges.** ε – average electron energy; τ_{rise} – pulse rise time; τ_f – pulse fall time; τ_{pd} – pulse duration; τ_{ε} – time for electron energy relaxation due to quasi-neutral plasma formation and the loss of high-energy electrons to the anode; τ_{rec} – recombination time of O atoms.

The use of plasma discharges for nanoscale synthesis is a rapidly developing field[1,14]. In particular, non-thermal plasmas (for which the mean electron energy $<\varepsilon>$ is significantly higher than the energy of neutral gas particles) at atmospheric pressure are attractive because of several factors conducive to efficiency[17,18]. Operating at atmospheric pressure eliminates the need for vacuum equipment and enables fast chemistry due to high species densities, thus speeding up growth compared to low-pressure synthesis. Non-thermal plasmas efficiently channel energy towards generating plasma chemical species such as electrons, ions, excited neutral species, and radicals typically not found in other synthesis environments that can serve as vehicles for the specific transfer of energy towards growth processes. So far, little attention has been paid to efficiency until recently[19,20].

Among non-thermal atmospheric-pressure plasma sources, nanosecond repetitive pulsed (NRP) discharges possess particularly high mean electron energy $<\varepsilon>$ and therefore may be well suited for efficient synthesis because significant fractions of the discharge energy are channeled to the electron-impact processes of ionization, electronic excitation, and dissociation when $<\varepsilon>$ is much greater than 1 eV. This subject has been explored previously in a perspectives article[19]. NRP discharges are generated by applying high-voltage nanosecond-duration pulses at high pulse repetition frequency (PRF), as shown in Figure 2. A short rise time minimizes electron-heavy species collisions at low $<\varepsilon>$ before high $<\varepsilon>$ is attained once the voltage reaches its maximum value. A recent model shows that $<\varepsilon>$ at atmospheric pressure increases up to a maximum value within several nanoseconds of the instantaneous application of a high-voltage pulse and then remains close to the maximum for
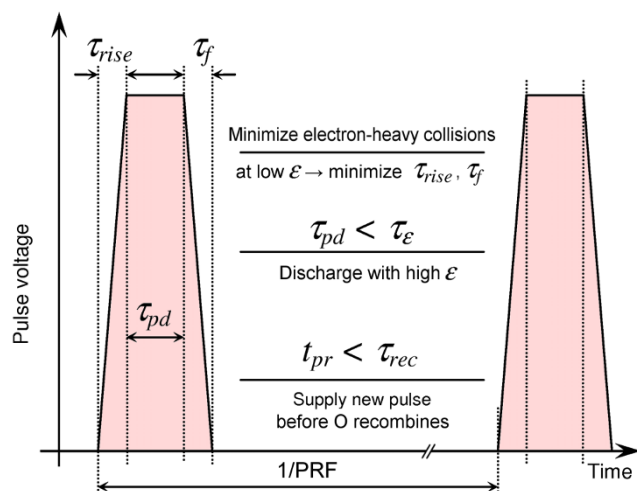
several tens of ns[21]. However, $<\varepsilon>$ then decreases significantly once a quasi-neutral plasma column forms. Thus, we aim to choose the pulse duration to maximize $<\varepsilon>$ while allowing sufficient time for synthesis. To maintain an active medium between pulses, the PRF is chosen to match the recombination time of the discharge. In practice, the above criteria can be met in air at atmospheric pressure using pulses with nanosecond-scale duration and rise time, with PRF of about 10 – 100 kHz, at applied voltages on the order of 10 kV for inter-electrode gaps on the order of 1 cm.

To test the ideas proposed in Refs. 1 and 19 that plasmas and NRP discharges in particular can be potentially used for targeted and efficient use of energy and matter in nanoscale synthesis, here we employ NRP spark discharges for controlling the production of metal and oxygen atoms in open ambient air, resulting in the synthesis of high quality MO$_3$ nanostructures suitable for various applications. When metal electrodes for plasma generation also serve as the source for metal precursor atoms, it is convenient to use spark discharges because they generate temperatures high enough for evaporating metal[22–24]. NRP spark-based nanofabrication consumes potentially much less energy than other methods while operating in open ambient air without catalysts or additional heating of the substrate. Furthermore, it is possible to synthesize on plastic, which is useful for hybrid organic-inorganic energy conversion and electronic devices. The high $<\varepsilon>$ of NRP discharges is a basic plasma property that may be generally useful in nanoscale synthesis and materials processing.

In this work, NRP spark discharges have been generated in open ambient air using two different vertical discharge configurations, as shown in Figure 1 as well as in Figure SI1 in Supplementary information. Details of the experimental setup are discussed in the Methods section.

Results

Metal-oxide nanoarchitectures – morphological, compositional, and structural characterization. Figure 3 is a selection of scanning electron microscopy (SEM) images showing a variety of nanostructures that have been synthesized using NRP spark discharges. Figures 3(a)–(e) show the nanostructures grown using the pin-to-pin setup (Fig. 1(b)) using an applied voltage of 5 kV and a pulse width of 45 ns. These nanostructures were collected via "remote
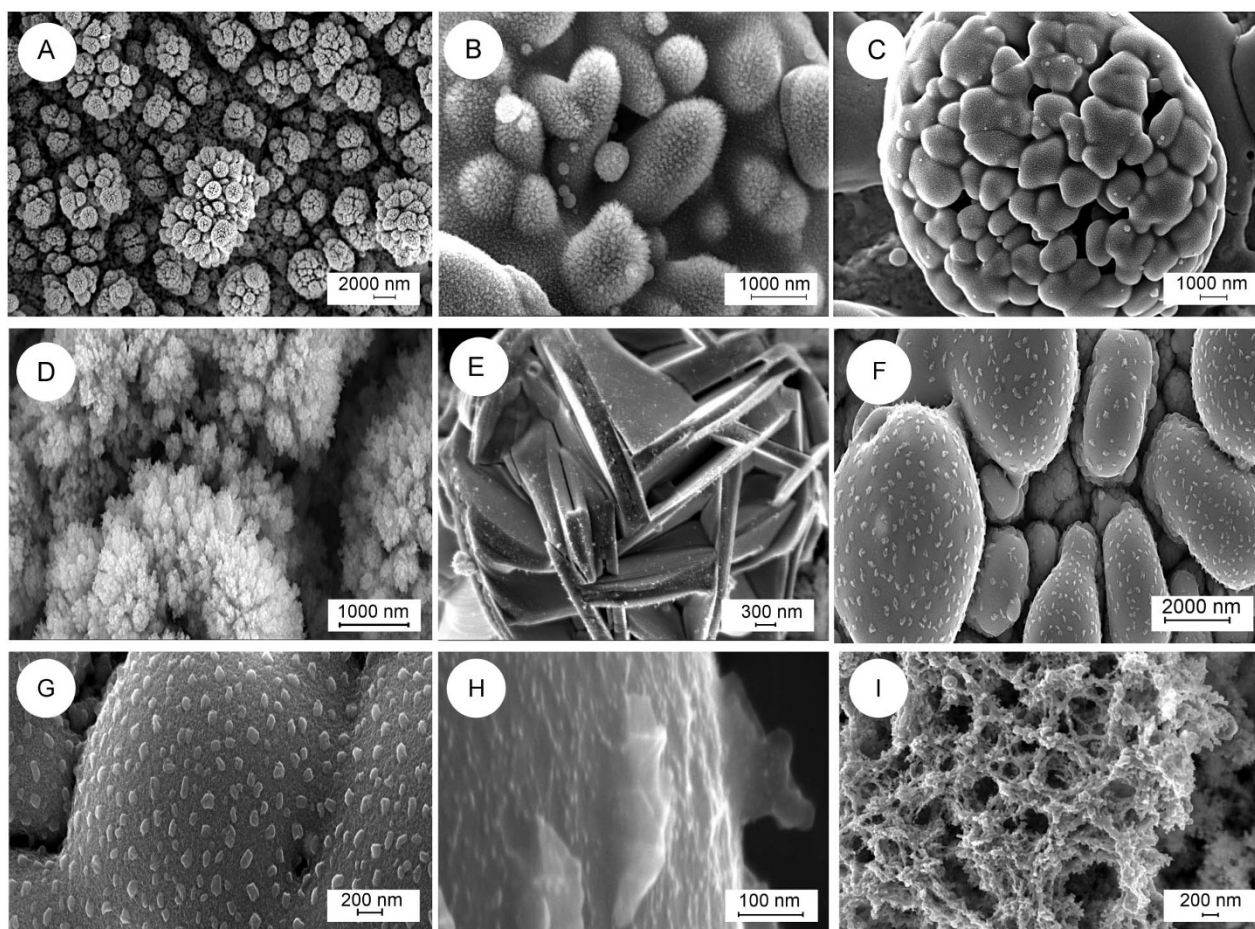
2

Figure 3 | SEM images of MoO₃ nanostructures. (a–e) Deposited in the pin-to-pin electrode configuration, (f–h) deposited in the pin-to-plate electrode configuration; (i) porous networks of MoO₃ deposited in the pin-to-plate configuration.

deposition" on different areas of copper strips attached to the inside surface of the plastic tube. As one can see from these images, the spark discharge forms hierarchical architectures with nanometer-scale flakes covering sub-micron scale features, which in turn form micron scale clusters. When the applied voltage was increased to 12 kV, the nanowall-like structures shown in Fig. 3(e) were formed. Figure 3(f)–(h) are the progressively enlarged views of the nanostructures grown using the pin-to-plate configuration shown in Fig. 1(c) at an applied voltage of 7.7 kV and a pulse width of 45 ns. In this case, hierarchical structures consisting of nanoscale dots studding the surfaces of micron-scale structures were also formed. Figure 3(i) shows a nanoporous network produced under the same conditions but at a location on the plane that is approximately 100 μm away from the spot at which the discharge contacts the cathode. In all cases, the produced nanostructures possess well-defined architectures (i.e. flakes, dots, walls, or a porous network), a reasonable uniformity in terms of their distribution over the micron-scale surfaces, and a well-defined structural hierarchy from the nanometer to micron scales.

Figure 4 shows more extensive results from materials characterization measurements. The energy-dispersive x-ray spectroscopy (EDS) spectrum from Figure 4(a) reveals the presence of Mo and O but the absence of N, indicating that oxides have been produced selectively by the discharge. As will be discussed later, NRP spark discharges can achieve up to 50% dissociation of O_2, and therefore it is reasonable to suspect that the abundance of O atoms leads to high oxide content. However, it is not possible to conclude that the lack of nitrides is due to the absence of N atoms, whose production may also be quite significant due to the dissociation of N_2 via electron impact[25].

Figure 4(b) shows a typical Raman spectrum for the nanoflakes shown in Figure 3(a) acquired using a probe beam size of ~ 1 μm. The presence of sharp bands is consistent with crystallinity, whereas the broad features upon which these sharp bands sit can be attributed to an amorphous phase[26,27]. The bands at 994, 821, and 664 cm^{-1} can be readily assigned to M=O and O–M–O stretch modes of α-MoO_3[28,29]. Smaller peaks at 774 and 849 cm^{-1} may be attributed to the same modes but for β-MoO_3[29]. The bands at 285 and 337 cm^{-1} can be assigned to the δ O=M=O wag mode common to both α- and β-MoO_3 and δ O–M–O bend mode of α-MoO_3, respectively. These bands are found not only in bulk MoO_3 but also in MoO_3 nano-structures[10,30]. Also, β-MoO_3 transforms to α-MoO_3 above 450°C[29], thus giving an idea of how hot the substrate surface must have been at some point during the synthesis process. Synthesis occurred on the polyamide substrate in this case, which did not suffer any noticeable thermal damage. This implies that the heat flux from the remote discharge was sufficient to create temperatures exceeding 450°C at the substrate surface but not throughout the bulk. Given the pulse train scheme used and the short duration of the NRP spark, it is possible that transient heating leads to such differences in bulk and surface temperatures of the substrate. Band positions may be shifted from those reported in the literature due to various effects, including different materials supporting the MoO_x nanostructures[31]. The absence of characteristic peaks for MoO_2 at 740 and 569/585 cm^{-1} is notable[32]. Finally, the band at 149 cm^{-1} corresponds to the strongest band of Cu_2O, which can be expected given that the substrate is Cu[33].

The conclusions drawn from the Raman spectrum are consistent with the x-ray photoelectron spectroscopy (XPS) spectrum shown in
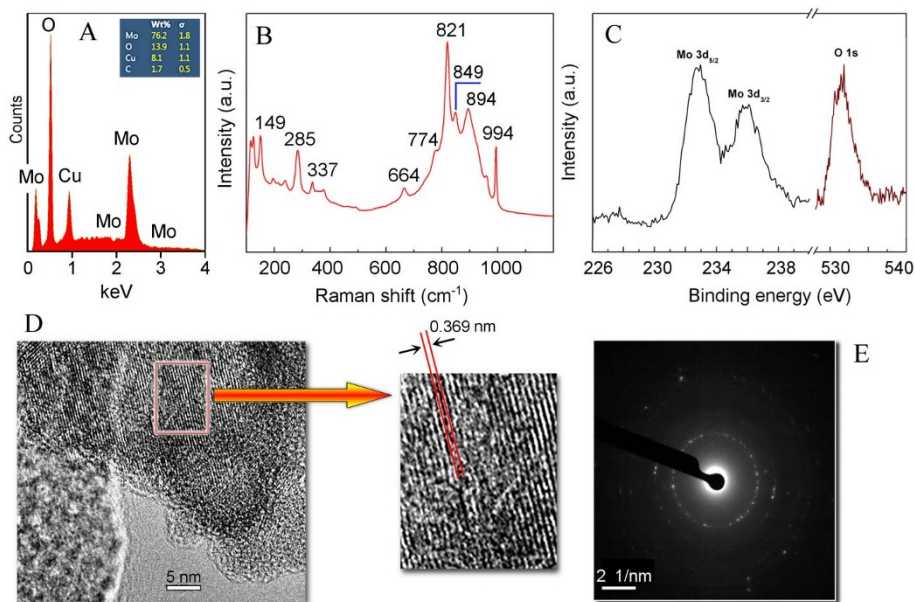
Figure 4 | Characterization measurements of the crystalline structure and chemical composition of the NRP spark-produced nanostructures shown in Figure 3(a). (a) Energy-dispersive X-ray (EDS) spectrum (b) Raman spectrum, (c) X-ray photoelectron (XPS) spectrum, (d) high-resolution TEM image, and (e) the corresponding selected area electron diffraction (SAED) pattern.

Figure 4(c). This spectrum shows peaks at 233 and 236 eV common to MoO_3 and MoO_2, but without the peak at 229 eV characteristic of MoO_2[34]. The high-resolution TEM image shown in Figure 4(d) demonstrates that a fraction of the domain is made of small nanocrystals, where the lattice spacing of 0.369 nm corresponds to the (001) plane of MoO_3[30]. Although not shown in Figure 4(d), lattice spacing of 0.345 nm corresponding to the (210) plane of MoO_3 is also observed[35]. A typical selected area electron diffraction (SAED) pattern collected from the sample is shown in Figure 4(e) and consists of concentric rings of resolved diffraction spots with few discrete spots lying outside the rings. Such a pattern indicates the presence of a single dominant phase consisting of relatively large polycrystalline grains that are randomly oriented[36]. This differs from the presence of both α- and β-MoO_3 indicated by Raman spectroscopy, which can be explained by the fact that the area probed by Raman spectroscopy is much larger than that probed by SAED. The first ring on the SAED pattern reveals the (002) plane of α-MoO_3.

Energy consumed in nanoscale synthesis. Figure 5 shows examples of single-shot measurements of the applied voltage, current, and discharge energy of the NRP spark discharges generated during synthesis. Unlike in previous work on NRP spark discharges[37], the total current here is considered to be the conduction current because the capacitance of the discharge circuit is much smaller in this work, such that we can consider the displacement current to be negligible. Single-shot measurements of the discharge energy E found by integrating the product of the current and voltage waveforms ranged from 1 to 8 mJ per pulse. This shot-to-shot variation is due to the discharge instability that can result from a variety of factors such as electrode erosion with each discharge event, and the fact that the NRP spark can require several pulses before initiating and then reaching stable behavior[37].

We can now estimate the energy cost per atom incorporated into the synthesized nanostructures (ε_{atom}). In addition to the aforementioned energy measurement, it was also observed that 2 ± 0.1 mm of the Mo anode was consumed using the direct deposition configuration. Note that in our experiment the peak current of up to 40 A well exceeds a threshold of 10–15 A required for hot spot formation, which means that a pure metal vapor was predominantly produced

in the spots formed on the electrode surface. Given that 600 pulse trains of 500 pulses each were applied, and assuming 1 – 8 mJ of energy was dissipated with each pulse, we have 300 – 2400 J of energy dissipated. Given that the Mo electrodes were 250 μm in diameter with 2 mm in length consumed, and that the mass density of solid Mo at room temperature is 10.28 g/cm³, with an atomic weight of
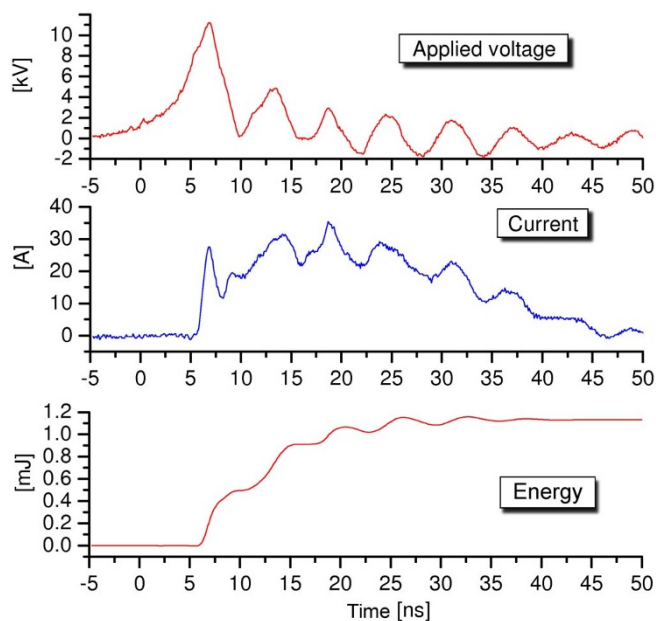

Figure 5 | Example of single-shot measurements of the applied voltage and current for the NRP spark discharge during the synthesis of the MoO_3 nanostructures shown in Figure 3, as well as the discharge energy calculated using these voltage and current waveforms. Note that although the pulse generator was set to deliver high-voltage pulses of 12.5-kV amplitude and 40-ns duration at PRF = 30 kHz, the low discharge resistance causes the voltage pulse to collapse upon spark development. See Figure SI2 in Supplementary information for a profile of an undistorted pulse.

95.94 g/mol, we thus assume here that 1 mg or 10 μmol of Mo has been incorporated into nanostructures. This amounts to about 300 – 2400 eV/atom of Mo. The nanostructures have been determined to be MoO_3 in the previous section, which yields $\varepsilon_{atom} = 75 – 600$ eV/atom.

Discussion

Now we consider ε_{atom} as a figure of comparison for the energy efficiency of various methods of nanomaterials synthesis. Globally speaking, it is the energy needed for producing atoms of building material (e.g. by dissociation or evaporation), transporting them to the stacking point, and overcoming energy barriers to incorporation into the assembly. On Table 1, we show the minimum possible $\varepsilon_{atom} = P/\dot{m}$ calculated for several studies of nanofabrication using atmospheric pressure plasma sources without external substrate heating, where P is the discharge power and $\dot{m}$ is the nanomaterial mass production rate. Details on how these quantities have been determined from the data in the references can be found in Ref. 19. For the case of the NRP sparks studied here, P and $\dot{m}$ are average values over 610 s in real time of applying discharges in the previously mentioned pulse-train fashion, although it should be noted that the instantaneous power during a pulse can reach over 100 kW. We caution that $\dot{m}$ for all of the cases shown in Table 1 was determined by assuming that all of the material collected or evaporated from electrodes was comprised of or transformed into the reported nanomaterial. To compare ε_{atom} for plasma processing to conventional non-plasma synthesis, we also performed a carbon nanotube growth experiment using a typical thermal furnace process on a Fe-catalyzed silicon substrate, with a furnace heating-up time of 5 min at 6 kW and a growth time of 10 min at 500 W (Furnace OTF-1200X, MTI Corporation).

Of all of the methods shown in Table 1, nanofabrication using NRP discharges is the most energy efficient with the caveat that the values for ε_{atom} shown are the minimum for their respective processes. For NRP discharges, $\varepsilon_{atom} = 75 – 600$ eV/atom represents the range of values obtained from single-shot measurements, as discussed in the previous section and in Supplementary information. This represents a significant and possibly dramatic improvement over the current benchmark of 1000 eV/atom, although further measurements on the average value of ε_{atom} will be necessary.

Thus, Table 1 implies that NRP spark discharges are capable of setting a new standard for energy efficiency in nanoscale synthesis. As discussed in the introduction, this possibility was anticipated in Ref. 19 because NRP discharges at atmospheric pressure feature high $<\varepsilon>$ greater than 2 eV for pulse widths under 100 ns[21]. Synthesizing MoO_x nanostructures in air requires the production of O atoms, which can occur via several mechanisms in an air plasma[38]. One example that contributes significantly in NRP sparks is a two-step mechanism[39,40] in which free electrons elevate ground-state N_2 to various electronically excited states N_2^* (reaction (1)), which in turn dissociate O_2 upon impact (reaction (2)):

$$e + N_2 \rightarrow N_2^* + e \qquad (1)$$

$$N_2^* + O_2 \rightarrow N_2 + O + O \qquad (2)$$
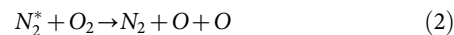
Reactions (1)–(2) illustrate the importance of high electron energy for efficiently producing O atoms. As $<\varepsilon>$ increases, a higher proportion of the electrons are found in the high-energy tail of the electron energy distribution function (EEDF), towards energies at which the cross-sections for useful processes is higher. As discussed in the introduction, NRP discharges achieve such control of the EEDF by first rapidly increasing $<\varepsilon>$ using a short rise time and maintaining high $<\varepsilon>$ for a short duration on the order of 10 ns before decreasing due to the screening of the applied field by space charge.

The time evolution of the EEDF of nanosecond discharges has been modeled for the case of a fast ionization wave at 4 torr and shows the development of a significant high-energy tail[41]. The corresponding time profile of $<\varepsilon>$ closely follows that of the reduced electric field E/N, where E is the electric field and N is the gas density, with a lag of 0.5 ns. The characteristic time for electron energy relaxation varies directly with the gas density. At atmospheric pressure, $<\varepsilon>$ would therefore respond yet faster for the same E/N. Although the decrease of $<\varepsilon>$ closely tracks that of E/N during the fall time of the pulse, the high-energy tail relaxes more slowly because this portion of the EEDF is no longer in equilibrium with the field. As a result, reaction rates at a given E/N for excitation, dissociation, and ionization can differ between unsteady and stationary applied field conditions.

The high-energy tail of the EEDF characteristic of nanosecond discharges with high $<\varepsilon>$ shifts the channeling of discharge energy towards reactions (1) and (2) and away from processes that generally are too low in energy to dissociate O_2. One key example of such wasteful processes in air is the vibrational excitation of N_2, which consumes over 99% of the discharge energy at low $<\varepsilon>$ of about 1 eV[38]. Such a low $<\varepsilon>$ is typical of dc discharges in air at atmospheric pressure, for example[42]. The vibrational energy generally cascades down to heat the gas via vibrational-translational energy transfer and does not contribute to ionization or electronic excitation. On the other hand, the fraction of the discharge energy expended on all ionization, electronic excitation, and dissociation processes in air can exceed 90% at high values of the reduced electric field[25], which correspond to high $<\varepsilon>$ conditions. The above arguments are supported by measurements showing that NRP spark discharges in air at atmospheric pressure achieve up to about 50% dissociation of O_2 via the mechanism described by reactions (1) and (2)[43].

Table 1 | Energy cost of incorporating each atom into the nanostructure $\varepsilon_{atom} = P/\dot{m}$ using different atmospheric-pressure synthesis processes, where P is the average power coupled into the system and $\dot{m}$ is the average mass production rate. In all cases, no external substrate heating was used. Quantities marked by (*) have been calculated in Ref. 19 based on data given in the listed references

Source	Carrier gas	Excitation	Nanomaterial	P [W]	Max. $\dot{m}$ [μg/s]	Min. ε_{atom} [eV]	Ref.
Thermal furnace	Ar	-	Carbon nanotubes	5,000	1	1.2×10^8	This work
Microplasma	Ar	144 MHz	Si nanocrystals	35	0.017	600000*	17,44
Microplasma	Ar	450 MHz	MoO_3 nanosheets	31	1*	42000*	12
Microplasma	Ar	450 MHz	WO_3 nanoparticles	20	35*	1400*	45
Microsecond spark	Ar	2-μs spark following voltage ramp	Au nanoparticles	1.5*	2*	1500*	23
mw torch	Ar	2.45 GHz	Graphene	250	33	1000*	46
mw torch	Ar	2.45 GHz	Carbon nanotubes	400	7	7200*	47
DC arc	Ar	DC	Ag nanoparticles	120*	3	50000*	48
NRP spark	Air	40-ns pulse at PRF = 30 kHz	MoO_3 nanoflakes/nanowalls	0.5–4	1.6	75	This work

In conclusion, the deterministic approach to energy-efficient nanoscale synthesis has been achieved using NRP spark discharges in ambient air. MoO₃ nanostructures have been synthesized in an open, ambient air environment without using a gas chamber or additional heating of the substrates. Furthermore, the energy expended per atom incorporated into the nanostructure has been shown to be very low compared to many typical plasma and thermal nanoscale synthesis techniques such as CVD. Nanosecond discharges can achieve such energy efficiency because the average electron temperature is maximized with short pulsed excitation. As a result, the discharge energy is focused towards plasma-chemical processes that are useful for synthesis, such as the dissociation of O_2. These advantages of using NRP discharges for nanomaterials synthesis mark an advance towards the goals of energy efficiency and sustainability outlined in the Grand Energy Challenge by the U.S. Department of Energy[2].

There are also other interesting aspects to NRP spark-based synthesis. Fast heating and cooling may be responsible for the formation of nonequilibrium material phases, as discussed in Refs. 19,20. Although the nanostructures have formed in a variety of architectures, they are all composed of MoO_3. No MoO_2 or nitrides have been detected, which indicates a high degree of chemical selectivity for synthesis. Furthermore, it was possible to grow nanostructures on a polyamide substrate placed only a few millimeters away from the discharge, without melting it. Note that although the pulse train scheme and air cooling were chosen to prevent overheating of the polyamide, the heat flux from the discharge during remote deposition would nonetheless be expected to be much less than when the NRP spark is in direct contact with the substrate.

There are a number of ways to build upon the results of this work. The pulse duration and amplitude can be tuned to produce desired rates of metal evaporation and oxygen dissociation. In this work, the pulses were applied in trains with pauses in between as a precaution against overheating the polyamide substrate. If the pulses were applied continuously instead, or if the pulse repetition frequency were increased, then the growth rate could be increased above that reported in this work. Furthermore, arrays of discharges could be used to scale up production.

Methods

Electrical circuit and measurement. In both cases, a solid-state switch-based generator (FID Technology FPG20-30MKS50) supplied positive-polarity pulses of 12.5-kV amplitude and 40-ns duration at a pulse repetition frequency (PRF) of 30 kHz. These high-voltage nanosecond pulses propagated down a 100-Ω coaxial cable terminated by a 2-mm discharge gap in parallel with a matching box. The anode was Mo wire of 250-μm diameter that also served as the precursor material. In the case of "remote" deposition (Figure 1(b)), the cathode was a wire identical to the anode, with a Cu foil strip placed 3 mm away from the discharge serving as the substrate. This Cu foil strip was supported inside a 6-mm diameter polyamide tube, which was cooled by forced air. As an additional measure against heating the polyamide tube, the pulses were applied in trains of 500 pulses each for a total 600 trains, with a 1-s pause between trains. In the case of "direct" deposition (Figure 1(c)), the cathode was a polished Cu plate that also served as the substrate upon which nanostructures were grown and analyzed. A slow downward airflow coming from above the anode aided the downward trajectory of evaporated particulates towards the substrate. For consistency, the pulse train scheme was also applied for the direct deposition experiments, even though no polyamide tube was used. See Supplementary information for a detailed schematic of the synthesis apparatus as well as details of the measurement techniques for materials characterization and energy.

A 100-MHz bandwidth high-voltage probe (Lecroy PPE20 kV) was used to measure the voltage across the discharge gap. The discharge current was measured with a Prodyn coil current monitor (Model I 125 2 HF) with a 0.7 rise time.

Characterization of nanomaterials. The surface morphologies, composition analyses and the crystalline features of MoO_3 nanostructures were investigated using SEM (Zeiss Auriga SEM, operated at 4 kV), an Oxford X-max large area EDS SDD detector attached to the SEM, confocal micro-Raman spectroscopy (Renishaw inVia Raman microscope, with a 514 nm laser excitation source), X-ray photoelectron spectroscopy (Specs SAGE 150, Mg Kα source), and HRTEM (JEOL 3000F, operated at 300 kV). EDS analysis was performed on the sample size area ∼ 1600 μm².

The mass of synthesized nanomaterials was determined by the consumption of the wire anode, as follows. The electrode (Mo wire of 0.25-mm diameter) was uniformly

consumed from the flat end-face (circular area of 0.25-mm diameter). No erosion of the cylindrical side surface was noticed. The consumption was estimated by measuring the wire length before the experiment and after the application of 3×10^5 discharges (600 trains of 500 repetitive discharges). The typical consumption after 3×10^5 pulses was 2 mm in length, with a measurement error of 5%. The experiments were repeated several times with very similar consumption levels.

1. Ostrikov, K. Control of energy and matter at nanoscales: challenges and opportunities for plasma nanoscience in a sustainability age. *J. Phys. D-Appl. Phys.* **44**, 174003 (2011).
2. Yarris, L. (ed U.S. Department of Energy) (BESAC Subcommittee on Grand Challenges for Basic Energy Sciences, 2007).
3. Chen, Z. B. *et al*. Core-shell MoO₃-MoS₂ Nanowires for Hydrogen Evolution: A Functional Design for Electrocatalytic Materials. *Nano Lett.* **11**, 4168–4175 (2011).
4. Brezesinski, T., Wang, J., Tolbert, S. H. & Dunn, B. Ordered mesoporous alpha-MoO₃ with iso-oriented nanocrystalline walls for thin-film pseudocapacitors. *Nat. Mater.* **9**, 146–151 (2010).
5. Taurino, A. M. *et al*. Synthesis, electrical characterization, and gas sensing properties of molybdenum oxide nanorods. *Appl. Phys. Lett.* **88**, 152111 (2006).
6. Zhou, J. *et al*. Large-area nanowire arrays of molybdenum and molybdenum oxides: synthesis and field emission properties. *Adv. Mater.* **15**, 1835–1840 (2003).
7. Hu, S. & Wang, X. Single-walled MoO₃ nanotubes. *J. Am. Chem. Soc.* **130**, 8126–8127 (2008).
8. Satishkumar, B. C., Govindaraj, A., Nath, M. & Rao, C. N. R. Synthesis of metal oxide nanorods using carbon nanotubes as templates. *J. Mater. Chem.* **10**, 2115–2119 (2000).
9. Zach, M. P., Ng, K. H. & Penner, R. M. Molybdenum nanowires by electrodeposition. *Science* **290**, 2120–2123 (2000).
10. Ding, Q. P. *et al*. Molybdenum trioxide nanostructures prepared by thermal oxidization of molybdenum. *J. Cryst. Growth* **294**, 304–308 (2006).
11. Cai, L. L., Rao, P. M. & Zheng, X. L. Morphology-Controlled Flame Synthesis of Single, Branched, and Flower-like alpha-MoO₃ Nanobelt Arrays. *Nano Lett.* **11**, 872–877 (2011).
12. Mariotti, D., Lindstrom, H., Bose, A. C. & Ostrikov, K. Monoclinic beta-MoO₃ nanosheets produced by atmospheric microplasma: application to lithium-ion batteries. *Nanotechnology* **19**, 495302 (2008).
13. Osterwalder, N., Capello, C., Hungerbuhler, K. & Stark, W. J. Energy consumption during nanoparticle production: How economic is dry synthesis? *J. Nanopart. Res.* **8**, 1–9 (2006).
14. Ostrikov, K. Colloquium: Reactive plasmas as a versatile nanofabrication tool. *Rev. Mod. Phys.* **77**, 489–511 (2005).
15. Beilis, I. I. The nature of high voltage initiation of an electrical arc in a vacuum. *Appl. Phys. Lett.* **97**, 121501 (2010).
16. Anders, A. *Cathodic Arcs*. (Springer, 2008).
17. Mariotti, D. & Sankaran, R. M. Microplasmas for nanomaterials synthesis. *J. Phys. D-Appl. Phys.* **43**, 323001 (2010).
18. Nozaki, T. & Okazaki, K. Carbon nanotube synthesis in atmospheric pressure glow discharge: A review. *Plasma Process. Polym.* **5**, 300–321 (2008).
19. Pai, D. Z. Nanomaterials synthesis at atmospheric pressure using nanosecond discharges. *J. Phys. D.: Appl. Phys.* **44**, 174024 (2011).
20. Ostrikov, K. Nanoscale control of energy and matter in plasma-surface interactions: towards energy- and matter-efficient nanotech. *Physics of Plasmas* **18**, 057101 (2011).
21. Iza, F., Walsh, J. L. & Kong, M. G. From Submicrosecond- to Nano second-Pulsed Atmospheric-Pressure Plasmas. *IEEE Trans. Plasma Sci.* **37**, 1289–1296 (2009).
22. Pai, D. Z. *et al*. Atmospheric-pressure discharges for the fabrication of surface-based metal nanostructures. *IEEE Trans. Plasma Sci.* **39**, 2814–2815 (2011).
23. Tabrizi, N. S., Ullmann, M., Vons, V. A., Lafont, U. & Schmidt-Ott, A. Generation of nanoparticles by spark discharge. *J. Nanopart. Res.* **11**, 315–332 (2009).
24. Byeon, J. H. & Kim, J. W. Production of carbonaceous nanostructures from a silver-carbon ambient spark. *Appl. Phys. Lett.* **96**, 153102 (2010).
25. Popov, N. A. Fast gas heating in a nitrogen-oxygen discharge plasma: I. Kinetic mechanism. *J. Phys. D-Appl. Phys.* **44**, 285201 (2011).
26. Ajito, K., Nagahara, L. A., Tryk, D. A., Hashimoto, K. & Fujishima, A. Study of the photochromic properties of amorphous MoO₃ films using Raman microscopy. *J. Phys. Chem.* **99**, 16383–16388 (1995).
27. Lee, S. H. *et al*. Raman spectroscopic studies of electrochromic a-MoO₃ thin films. *Solid State Ion.* **147**, 129–133 (2002).
28. Dieterle, M., Weinberg, G. & Mestl, G. Raman spectroscopy of molybdenum oxides - Part I. Structural characterization of oxygen defects in MoO₃₋ₓ by DR UV/VIS, Raman spectroscopy and X-ray diffraction. *Phys. Chem. Chem. Phys.* **4**, 812–821 (2002).
29. Haro-Poniatowski, E. *et al*. Micro-Raman characterization of WO₃ and MoO₃ thin films obtained by pulsed laser irradiation. *Appl. Surf. Sci.* **127**, 674–678 (1998).
30. Hu, X. K. *et al*. Comparative study on MoO₃ and HₓMoO₃ nanobelts: Structure and electric transport. *Chem. Mat.* **20**, 1527–1533 (2008).
31. Mestl, G. & Srinivasan, T. K. K. Raman spectroscopy of monolayer-type catalysts: Supported molybdenum oxides. *Catal. Rev.-Sci. Eng.* **40**, 451–570 (1998).

32. Dieterle, M. & Mestl, G. Raman spectroscopy of molybdenum oxides - Part II. Resonance Raman spectroscopic characterization of the molybdenum oxides Mo_4O_{11} and MoO_2. *Phys. Chem. Chem. Phys.* **4**, 822–826 (2002).

33. Reimann, K. & Syassen, K. Raman scattering and photoluminescence in Cu_2O under hydrostatic pressure. *Phys. Rev. B* **39**, 11113–11119 (1989).

34. Choi, J. G. & Thompson, L. T. XPS study of as-prepared and reduced molybdenum oxides. *Appl. Surf. Sci.* **93**, 143–149 (1996).

35. Kim, M. R., Ahn, S. J. & Jang, D. J. Fabrication and characterization of MoO_3 clusters-coated TiO_2 nanotubes showing charge-transferred photoluminescence. *Eur. Phys. J. D* **52**, 75–78 (2009).

36. Williams, D. B. & Carter, C. B. *Transmission Electron Microscopy: A Textbook for Materials Science.* Second edn. (Springer, 2009).

37. Pai, D. Z., Lacoste, D. A. & Laux, C. O. Nanosecond repetitively pulsed discharges in air at atmospheric pressure – the spark regime. *Plasma Sources Science & Technology* **19**, 065015 (2010).

38. Becker, K. H., Kogelschatz, U., Schoenbach, K. H. & Barker, R. J. *Non-equilibrium Air Plasmas at Atmospheric Pressure.* (IOP Publishing, 2005).

39. Popov, N. A. Fast gas heating in a nitrogen–oxygen discharge plasma: I. Kinetic mechanism. *J. Phys. D-Appl. Phys.* **44**, 285201 (2011).

40. Rusterholtz, D. L., Pai, D. Z., Stancu, G. D., Lacoste, D. A. & Laux, C. O. in *50th AIAA Aerospace Sciences Meeting*, AIAA 2012–0509 (Nashville, Tennessee, 2012).

41. Starikovskaia, S. M. & Starikovskii, A. Y. Numerical modelling of the electron energy distribution function in the electric field of a nanosecond pulsed discharge. *J. Phys. D-Appl. Phys.* **34**, 3391–3399 (2001).

42. Nagulapally, M. *et al.* in *31st AIAA Plasmadynamics and Lasers Conference* Vol. AIAA Paper 2000–2417 (Denver, Colorado, 2000).

43. Stancu, G. D., Kaddouri, F., Lacoste, D. A. & Laux, C. O. in *40th AIAA Plasmadynamics and Lasers Conference* Vol. AIAA Paper 2009–3593 (San Antonio, 2009).

44. Nozaki, T., Sasaki, K., Ogino, T., Asahi, D. & Okazaki, K. Microplasma synthesis of tunable photoluminescent silicon nanocrystals. *Nanotechnology* **18**, 235603 (2007).

45. Shimizu, Y. *et al.* Reactive evaporation of metal wire and microdeposition of metal oxide using atmospheric pressure reactive microplasma jet. *Jpn. J. Appl. Phys. Part 1-Regul. Pap. Brief Commun. Rev. Pap.* **45**, 8228–8234 (2006).

46. Dato, A., Radmilovic, V., Lee, Z. H., Phillips, J. & Frenklach, M. Substrate-free gas-phase synthesis of graphene sheets. *Nano Lett.* **8**, 2012–2016 (2008).

47. Chen, C. K., Perry, W. L., Xu, H. F., Jiang, Y. B. & Phillips, J. Plasma torch production of macroscopic carbon nanotube structures. *Carbon* **41**, 2555–2560 (2003).

48. Chen, J. H., Lu, G. H., Zhu, L. Y. & Flagan, R. C. A simple and versatile mini-arc plasma source for nanocrystal synthesis. *J. Nanopart. Res.* **9**, 203–213 (2007).

Acknowledgements

Author contributions

D.Z.P. and K.O. conceived the project and co-wrote the manuscript. D.Z.P. led the project, designed and performed the synthesis experiments, and analyzed all the data. K.O. supported the work and provided guidance and ideas. S.K. performed the materials characterization and analyzed the corresponding data. D.A.L. performed additional discharge characterization experiments. I.L. contributed to the results interpretation and manuscript preparation. C.O.L. supported the work and contributed to manuscript preparation. All authors discussed the results and read the manuscript.

Additional information

Supplementary information accompanies this paper at http://www.nature.com/scientificreports

Competing financial interests: The authors declare no competing financial interests.

How to cite this article: Pai, D.Z. *et al.* Energy efficiency in nanoscale synthesis using nanosecond plasmas. *Sci. Rep.* **3**, 1221; DOI:10.1038/srep01221 (2013).